JOURNAL OF AIRCRAFT
Vol. 38, No. 2, March–April 2001

Suppression of Pressure Oscillations in High-Mach-Number, Turbulent, Cavity Flow

S. W. Perng* and D. S. Dolling†
University of Texas at Austin, Austin, Texas 78712-1085

Fluctuating wall pressure measurements have been made in a high-Reynolds-number, Mach 5, turbulent cavity flow. The cavity length to depth ratio was varied from 3 to 5 with a fixed width to depth ratio of 3. Slotted and vented upstream and downstream walls, slanted downstream walls (inclined in either the streamwise direction only or inclined streamwise and swept spanwise), and spoiler and vortex generator arrangements were used to explore their effectiveness at suppressing the pressure oscillations. In practice, wall geometry will be dictated by many constraints; thus, in the absence of a particular application, it is not meaningful to claim that one particular geometry is the most effective. However, consistent with work at lower Mach numbers, it is evident that certain slanted and swept downstream walls are quite effective, reducing the high mean pressure and rms pressure levels near the downstream wall/floor junction by 30–35% and 40%, respectively. At this high Mach number, the coupling between the shear layer dynamics and cavity acoustics is weak. As a consequence, the cavity mode frequencies, which are essentially independent of geometry changes, are in as good an agreement with closed-box frequency predictions as they are with the predictions of Rossiter's modified formula (Rossiter, J. E., "Wind Tunnel Experiments on the Flow over Rectangular Cavities at Subsonic and Transonic Speeds," Aeronautical Research Council Reports and Memoranda, ARCR & M No. 3438, London, 1964).

Nomenclature

a	=	sonic speed
C_f	=	skin-friction coefficient
f	=	frequency, Hz
$G(f)$	=	power spectral density
H	=	cavity depth
k_c	=	U_c/U_∞
L	=	cavity length
M	=	Mach number
n	=	mode number
P	=	wall pressure
r	=	recovery factor
Re	=	Reynolds number
T	=	temperature
t	=	time
U, U_c	=	local mean velocity, convection velocity
W	=	cavity width
x, y, z	=	streamwise, vertical, and spanwise coordinates
α	=	phase constant between vortex shedding and acoustic wave response in cavity
γ	=	specific heat ratio
δ	=	boundary-layer velocity thickness
δ^*	=	boundary-layer displacement thickness
θ	=	boundary-layer momentum thickness
Π	=	wake strength
ρ	=	density

Subscripts

0	=	stagnation
∞	=	freestream

Received 2 February 2000; revision received 5 September 2000; accepted for publication 5 September 2000.

*Graduate Student, Department of Aerospace Engineering and Engineering Mechanics, Center for Aeromechanics Research; currently Associate Professor, Chung-Cheng Institute of Technology, Yuanlin Li, Dashi Jen, Taoyuan County, 33509, Taiwan, Republic of China.

†Professor, Department of Aerospace Engineering and Engineering Mechanics, Center for Aeromechanics Research. Fellow AIAA.

Introduction

INTERNAL carriage of stores offers many benefits for transonic and supersonic military aircraft including elimination of store aerodynamic heating, reduction of aircraft drag and radar signature, greater maneuverabiltiy, and enlarged flight envelope. However, flight data and extensive experimental and computational studies over the past 40 years have shown that airflow past cavities, such as aircraft weapons bays, can induce intense, self-sustaining, pressure oscillations in and around the cavity. A review of much of the early work in subsonic and supersonic flows was compiled by Charwat et al. in 1961.[1] In the late 1970s Rockwell and Naudascher[2] published a detailed review of 78 studies in which they developed a general framework for describing the various flow types. A less detailed review, but one which includes work of the 1980s and early 1990s, may be found by Perng.[3]

Fluctuating pressure loads on the downstream wall and at the junction of the downstream wall and cavity floor can be severe. Computations[4] and experiments[3] show that peak fluctuating levels can be as high as 2–3 times the freestream static pressure P_∞, with overall sound pressure levels (OASPLs) of 160 dB or more. To protect stores and interior bay structure from damage, methods are needed for suppressing the pressure oscillations. In Ref. 3, Perng provides a brief review of some of the work that has been done in this area, including active and passive approaches. Active approaches have included steady and pulsating injection and oscillating fences. Vakili and Gauthier[5] used high- and low-density upstream injection for a cavity with $L/H = 2.54$, $W/H = 1$, and $\delta/H = 0.17$ at $M_\infty = 1.8$ and found that low-density injection was very effective; amplitude reductions of up to 27 dB were obtained. Later work by Vakili et al.[6] at $M_\infty = 0.7$ and 1.75 with $L/H = 4.3$ employed five different porous injection plates and similarly impressive results were reported. Sarno and Franke[7] used static and oscillating fences and steady and oscillating injection at the cavity leading edge ($L/H = 2$ and $W/H = 0.3$) for M_∞ from 0.6 to 1.5. Fence oscillation frequencies (maximum of 220 Hz) and injection frequencies (<70 Hz) were small compared to the first mode frequency (≤1.6 kHz). Although injection was quite effective, with a 45-deg angle preferable to parallel injection, the static fence was most effective; with a fence height greater than δ and at $M_\infty = 1.28$, the amplitude of the first mode was decreased by about 30 dB.

Based on the preceding examples, significant loading reduction using active control is clearly feasible. Whether active control is the best solution for any given application will clearly depend on the severity of the loading, the magnitude of the reduction that the design criteria dictate, the ensuing complexity, and cost. In a general sense, a passive control technique, with no moving parts and with no need to move (or modulate) large volumes of gas, will probably be less expensive and easier to implement and maintain. Accordingly, many passive methods have been explored over the years including vortex generators[8] and slanted downstream walls,[8,9] venting chambers,[10] leading-edge saw-tooth suppressors[11,12] (including experiments on a model of an F-111 bomb bay), and leading edge pins[13] and spoilers.[9] Because the same device may produce suppression or amplification depending on the arrangement and flow conditions, it is difficult to draw broad-based conclusions. As an example of the magnitude of the possible suppression, Heller and Bliss[8] found that at Mach 0.8 and $L/H = 2.3$, a combination of a slanted downstream wall and detached cowl just upstream of the downstream wall reduced the amplitude of the dominant frequency by about 23 dB. Wilcox's venting chamber[10] was designed to let high-pressure air at the downstream of the cavity vent to the lower pressure region at the upstream end. Cavity drag was reduced as much as 50%, but the required volume of the venting chamber was comparable to that of the cavity itself. The experiments of Clark et al. at Mach numbers from 0.6 to 3.0 and L/H from 5 to 10 included saw-toothed and perforated fences to deflect the shear layer away from the cavity.[11] In supersonic flow, the perforated fence was more effective than the saw-toothed fence. The leading-edge saw-toothed suppressors used by Shaw et al.[12] on a 4.9% scale model of an F-111 aircraft ($L/H = 6.79$ and 10.27) were tested at subsonic and supersonic speeds and "were partially effective in suppressing the tones. In some cases the levels were amplified." They found that an aft bulkhead inclined at 48 deg was "very effective in suppressing the levels."

In the current experimental study, carried out at Mach 5, the focus is also on passive methods, in particular geometry changes to the downstream wall. The walls included slotted and vented geometries, used as both upstream and downstream walls, as well as slanted walls. The latter included walls inclined streamwise only, as well as walls with a combination of streamwise and spanwise sweep. A particularly interesting question was whether walls inclined streamwise, which have been shown to be effective at lower Mach numbers, would be equally effective at high Mach number where the coupling between the shear layer dynamics and the cavity acoustics is much weaker. The experiments were carried out in open cavity flow, that is, shear layer reattaches on the downstream wall, using a cavity with a length to depth ratio L/H equal to 3 or 4, width to depth ratio W/H fixed at 3, and boundary layer to depth ratio δ/H of about 0.76. The ratios L/H and δ/H are low and high, respectively, compared to a typical weapons bay application, and thus, this study was not an attempt to provide data for engineering design. Sinha et al.[14] have reviewed the pros and cons of Reynolds averaged Navier–Stokes (RANS) modeling and large eddy simulation (LES) of open cavity flows. RANS is found to be too dissipative, that is, it suppresses the acoustic field and underpredicts dynamic loads, whereas LES has the potential to provide a credible prediction of dynamic loads. The current results, which show how the mean and fluctuating loads (and spectra) are systematically affected by geometry changes, should prove particularly useful in the assessment of such predictions as they become more commonplace over the next few years.

Experimental Facility, Models, and Instrumentation

Wind Tunnel

The experiments were conducted in the Mach 5 blowdown tunnel of the University of Texas at Austin. The test section is 17.78 cm high $\times$ 15.24 cm wide $\times$ 76.2 cm long. About 4 m^3 of air stored in tanks at 17 MPa gives a run time of approximately 70 s. Upstream of the stagnation chamber, the air is heated by two 420-kW electric resistive heaters. The stagnation pressure and temperature for all experiments were 2.29 MPa $\pm$ 15 kPa and 357 $\pm$ 4 K, respectively.

Table 1 Incoming flow conditions and boundary-layer properties

Property	Value
M_∞	4.95
U_∞	765 m/s
Re_∞	5.0×10^7/m
P_0	2.29×10^6 Pa
T_0	357 deg K
δ	1.93 cm
δ^*	0.91 cm
θ	0.076 cm
Π	0.44
C_f	7.6×10^{-4}

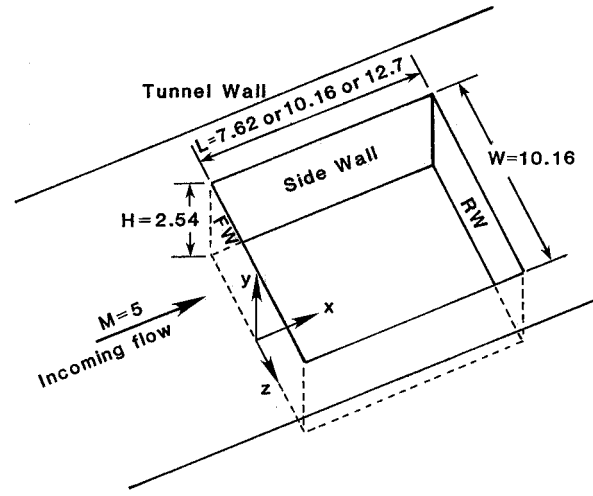

Fig. 1 Cavity dimensions and coordinate system.

The incoming tunnel floor boundary layer undergoes natural transition far upstream of the nozzle exit and develops under approximately adiabatic wall temperature conditions. The nominal properties of the incoming freestream and undisturbed turbulent boundary layer on the centerline of the tunnel are given in Table 1. The displacement thickness δ^* and the momentum deficit thickness θ were determined from the profiles of u/U_∞ and ρ/ρ_∞ calculated from pitot surveys assuming an adiabatic wall and constant static pressure normal to the tunnel wall. The velocity profiles were good fits to the law of the wall–law of the wake.

Cavity Model

The cavity model was designed in modular form so that the rectangular upstream and downstream walls of the baseline case could be easily replaced with different geometries. Details of the design are given in Ref. 3. The width W and height H were held fixed at 7.62 and 2.54 cm, respectively while the length L could be varied from 7.62 to 12.70 cm. The coordinate system employed is shown in Fig. 1. The origin is at the midpoint of the front wall, at the bottom, with the x direction downstream, y perpendicular to the tunnel floor, and z spanwise. The cavity upstream wall is 47.5 cm downstream of the wind-tunnel nozzle exit plane. Seven walls were tested in two phases. In phase 1, vented, slotted, slanted, and beak (named based on its resemblance to a bird's beak) walls were tested. Based on the success of the slanted and beak walls, two more walls with different slant angles were used in phase 2. In addition, largely out of curiosity, a wall with reverse features to the beak (named the valley wall) was also used. They are described briefly subsequently. To accommodate future researchers who may wish to compute these flows, complete geometric details are provided in Fig. 2.

Vented and Slotted Walls

In open cavity flow, the highest mean pressures occur near the floor/downstream wall junction and on the downstream wall. With

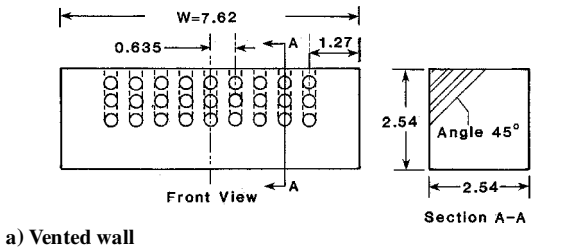

a) Vented wall

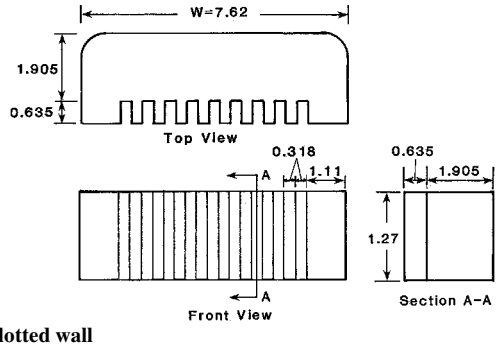

b) Slotted wall

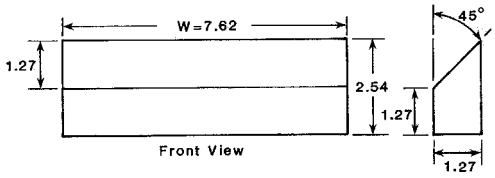

c) Slanted wall

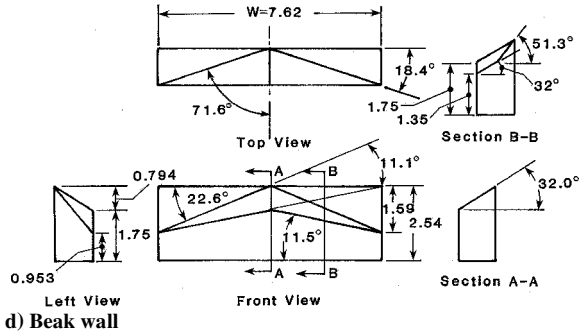

d) Beak wall

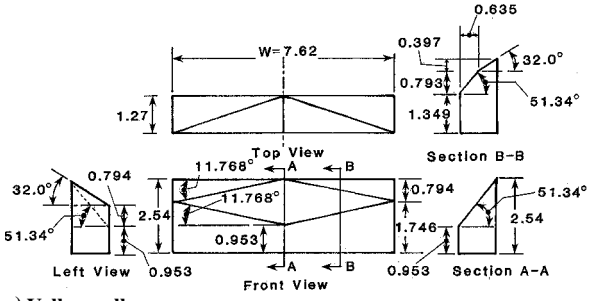

e) Valley wall

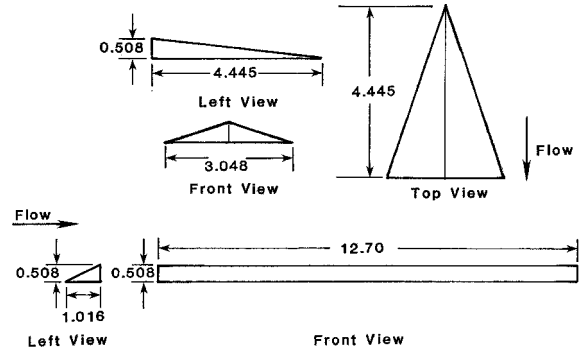

f) Vortex generator and wedge spoiler

Fig. 2 Wall, vortex generator, and spoiler geometries (dimensions in centimeters).

the vented geometry (Fig. 2a), 27 circular ducts of diameter 0.318 cm were drilled in the upper part of the downstream wall. The upper, middle, and lower rows of holes were located 0.318, 0.794, and 1.27 cm, respectively, from the top of the wall. It was anticipated that the large pressure difference (approximately $0.4 - P_\infty$, depending on position) between the downstream wall and the tunnel floor surface downstream of this wall would force some fraction of the high-pressure air out of the cavity. It was thought this would reduce the scale and intensity of the trailing-edge vortex and lower the amplitude of the pressure oscillations. Shaw et al.[12] conducted experiments at Mach numbers from 0.9 to 2.0 in which there was a slot in the downstream wall of the cavity. The slot, which was about 40% of the width of the cavity, housed a sting that supported a store model. Depending on flow conditions, the slot reduced the amplitude of modes 2 and 3 from 5 to 8 dB. Thus, the slotted wall (Fig. 2b) was an attempt to see if a series of nine smaller span slots would be an effective suppression device. There was also some thought that an irregular surface might also attenuate the forward-propagating acoustic wave originating at the downstream wall or influence the reflection of an incoming acoustic wave at the upstream wall. Hence, both the vented and slotted walls were also used as an upstream wall.

Slanted Wall

Rockwell and Knisely's flow visualization experiments[15] in a water tunnel ($L/H = 2$) showed that the vortices shed from the upstream wall underwent three types of impingement at the downstream wall: complete, or partial clipping, or complete escape. Infinite fringe interferograms have also shown that partial clipping can occur[16] in supersonic flow. If partial clipping can be enhanced, then less high-energy air will flow into the cavity, and pressure fluctuation amplitudes should be smaller. Thus, the slanted wall (Fig. 2c), used only as a downstream wall, was designed to decrease the shear layer impingement angle with the hope of allowing a larger fraction of high-energy air to escape the cavity. As noted earlier, Shaw et al.[12] used a 48-deg slanted downstream wall at Mach numbers of 0.9 and 1.2 and obtained significant suppression. In phase 1, a single slanted wall with an angle of 45 deg to the vertical was used. This wall is referred to as RW1. In phase 2, two additional walls with angles of 38.7 deg (RW2) and 30.2 deg (RW3) to the vertical were used. With the latter, the inclined surface terminated 0.96 and 0.36 cm, respectively, above the cavity floor.

Beak and Valley Wall

In a regular cavity with four vertical walls, lateral vortices are formed near the upstream edges of the sidewalls, probably induced by the pressure difference between the cavity and freestream.[4,17] Because of side-wall friction and these lateral vortices, the pressure at the sides of the downstream wall tends to be lower than on centerline; thus, there is a natural tendency for flow to move spanwise along the downstream wall. The beak wall with its combination of streamwise slant and spanwise sweep (Fig. 2d) was designed to increase the mass of fluid swept to the cavity sides. The valley wall (Fig. 2e), so named because the center is cut deeper than the edges, is essentially the reverse geometry of the beak wall in which flow is induced to flow from the edges to the centerline.

Boundary-Layer Spoilers/Manipulators

As noted earlier, experiments have shown that spoilers placed upstream of the cavity can suppress pressure oscillations.[11,12] Such techniques have also been explored computationally. Baysal et al.[18] computed the transonic ($M_\infty = 0.95$) flow over a cavity ($L/H = 4.5$) with a vertical spoiler at the leading edge and found that on the cavity floor the dominant modes were suppressed by about 15 dB. In the current study, three Wheeler-type[19] vortex generators (one of which is shown in Fig. 2f) and a small wedge (Fig. 2f) were placed close to the upstream wall of the cavity. Barter[20] has used these generators in the same Mach 5 boundary layer as in the current experiment and shown that they produce momentum deficient regions downstream of the apexes with a corresponding local thickening of the boundary layer, as well as increased turbulence levels in the boundary layer.

The full-span wedge was placed with its trailing edge 2.54 cm upstream of the cavity. The wedge corner angle of 26 deg was sufficient to separate the boundary layer and induce an unsteady separation shock upstream of the wedge.

Instrumentation and Data Acquisition

Fluctuating surface pressure measurements were made using Kulite Semiconductor Products, Inc., Model XCQ-062-15A and XCQ-062-50A transducers. The transducers have a nominal outer diameter of 0.16 cm and a pressure-sensitive diaphragm 0.071 cm in diameter. The transducers were installed flush with the cavity surface and were calibrated using a Heise digital pressure gauge, which is accurate to 7 Pa. Following calibration, the transducer voltages and the calibration pressure values were fitted to a straight line. The deviation of the calibration data points to the fitted line was typically within 0.5% using a least-squares curve fit. To minimize uncertainty, the transducers were calibrated at least twice each day. On the cavity floor, 19 transducer ports were available, of which 8 were off centerline to examine flowfield symmetry. Output from the transducers was amplified, low-pass filtered with the cutoff set at 25 kHz, and digitized at 50 kHz per channel using two LeCroy A/D converters, which are 12-bit accurate. A total of 512 records (524, 288 data points) were obtained for each channel. Data from the A/D memory buffers were downloaded to a workstation and stored on magnetic tapes for later analysis.

Discussion of Results

Mean and Fluctuating Wall Pressures

Distributions of normalized mean pressure and standard deviation (and OASPL) on the cavity centerline for $L/H = 3$ and 4 for the baseline geometry, that is, four vertical walls, are shown in Figs. 3 and 4, respectively. The standard deviation is calculated for the bandwidth 0.34–25 kHz to eliminate noise from the electronics, which was centered around 180 Hz. Note that the lower cutoff is far from the cavity first mode frequency (around 2 kHz). On the abscissa, the upper edge of the front wall is at -1, with the front wall/cavity floor junction at 0. The shapes of the distributions for these baseline cases are as expected. The mean is relatively constant and close to P_∞ over much of the cavity floor, increasing toward the downstream wall/floor junction. The maximum mean pressure and standard deviation occur at the top of the downstream wall and result from the intermittent pressure signal caused by the transient shock that forms as the shear layer deflects in and out of the cavity or as individual large-scale shear layer structures impact the downstream wall.[21,22]

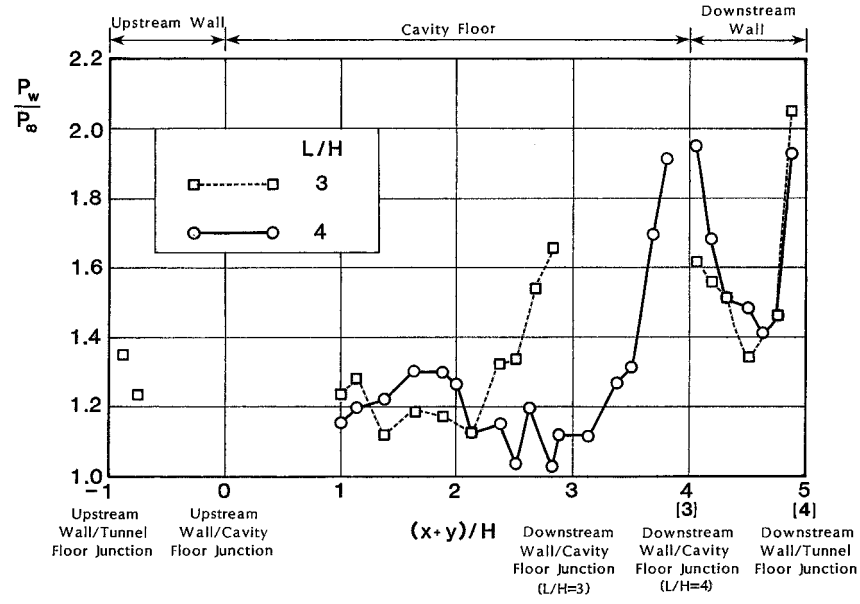

Fig. 3 Mean wall pressure distributions: baseline cavity, $L/H = 3$ and 4.

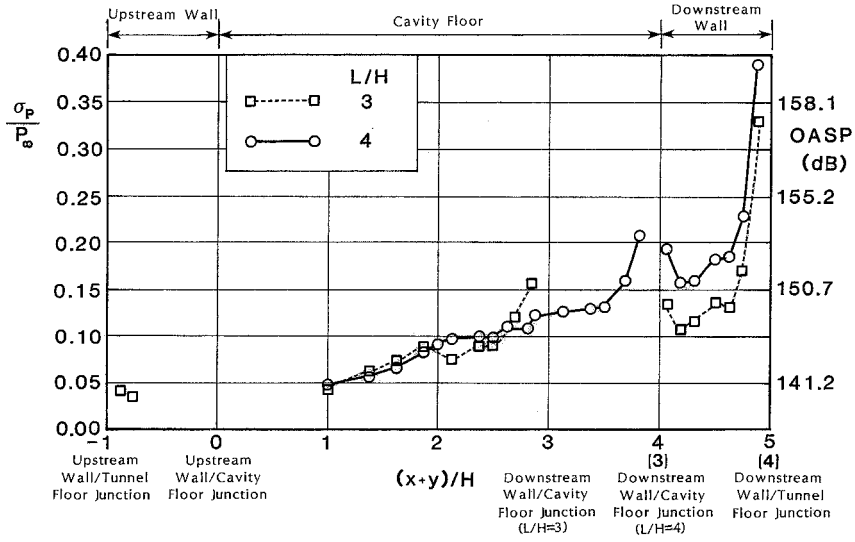

Fig. 4 Normalized wall pressure standard deviation and OASPL distributions: baseline cavity, $L/H = 3$ and 4.

Two 2-ms-long samples of the pressure signals at the top of the upstream wall (port FW1, location shown later) and downstream wall (port R7) for $L/H = 3$ show the intermittent character of the signal on the downstream wall (Fig. 5). Although the mean pressure at the top of the downstream wall is approximately $2P_\infty$, peak amplitudes are above $3P_\infty$. The OASPL distribution shows similar trends with a maximum value of 157–159 dB at the top of the downstream wall, about 10–15 dB higher than on the floor (Fig. 4).

The kerosene-diesel-lampblack method was used for surface flow. In this method the mixture is painted on the cavity internal surfaces and nearby tunnel floor. After tunnel shutdown, a full-scale, undistorted record of the mean wall shear direction is obtained by lifting the dried pattern off those surfaces on sheets of transparent tape. All three cavities ($L/H = 3$, 4, and 5) had similar flow features. Figure 6 shows a schematic from the flow visualization for $L/H = 4$. The flow is clearly three dimensional and is symmetric about the centerline. The measured mean pressure ratios (normalized by centerline values) on the downstream wall at $(x + y)/H = 3.875$ and $z/W = \pm 0.25$ were 1.04 and 1.03 for $L/H = 3$ and the corresponding normalized standard deviation ratios were 1.66 and 1.60, providing additional confirmation of symmetry. Note that the streaklines on the downstream wall are swept spanwise even with a rectangular geometry giving some indication that a symmetric, spanwise-swept wall (such as the beak) should be effective. The centerline flow structure inferred from Fig. 6 (and Figs. 3 and 4) is shown in Fig. 7. Figure 7 also shows the pressure port locations and designations.

Power spectra on the centerline at one station on the front wall $[(x + y)/H = -0.875]$, two on the floor $[(x + y)/H = 1.875, 2.81]$, and two on the downstream wall $[(x + y)/H = 3.31, 3.875]$ for the baseline case for $L/H = 3$ are shown in Fig. 8. The power spectral density $G(f)$ on the left-hand axis is in Pascal squared per Hertz, whereas sound pressure level (SPL) on the right is in decibels. The frequencies of the first three modes, f_1, f_2, and f_3, are quite evident, particularly on the upstream wall and near the downstream wall/floor junction and occur at approximately 2.15, 4.44, and 6.64 kHz, respectively. As expected, increasing the cavity length to $L/H = 4$ (and 5) reduced the first mode frequency to 1.66 (and 1.37) kHz, the second mode to 3.17 (and 2.54) kHz, and third mode to 5.32 (and 4.54 kHz). Furthermore, with longer cavities, the fourth mode was more evident and occurred at 7.13 kHz ($L/H = 4$) and 6.30 kHz ($L/H = 5$).

An interesting question is how effective Rossiter's method is for calculating mode frequencies at high supersonic Mach numbers.[23] Rossiter's formula, as modified by Heller and Bliss[8] is given by

$$\text{Strouhal number} = \frac{fL}{U_\infty} = \left[\frac{(n-\alpha)}{M/\sqrt{1+(r/2)(\gamma-1)M^2}+(1/k_c)}\right] \qquad n = 1, 2, 3, \ldots \quad (1)$$

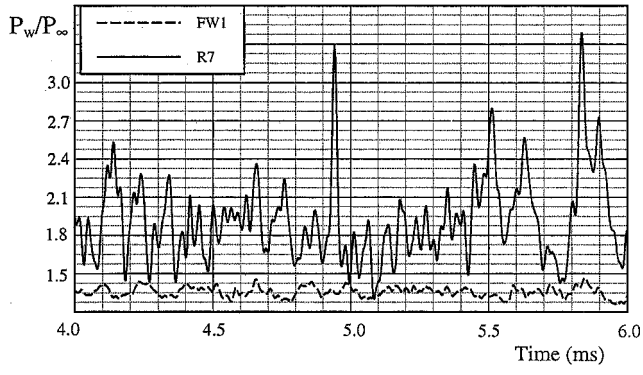

Fig. 5 Sample pressure signals on upstream (port FW1) and downstream (port R7) walls, *L/H* = 3.

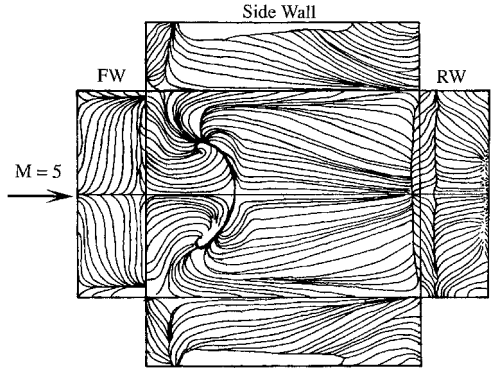

Fig. 6 Baseline surface flow visualization, *L/H* = 4: exploded view.

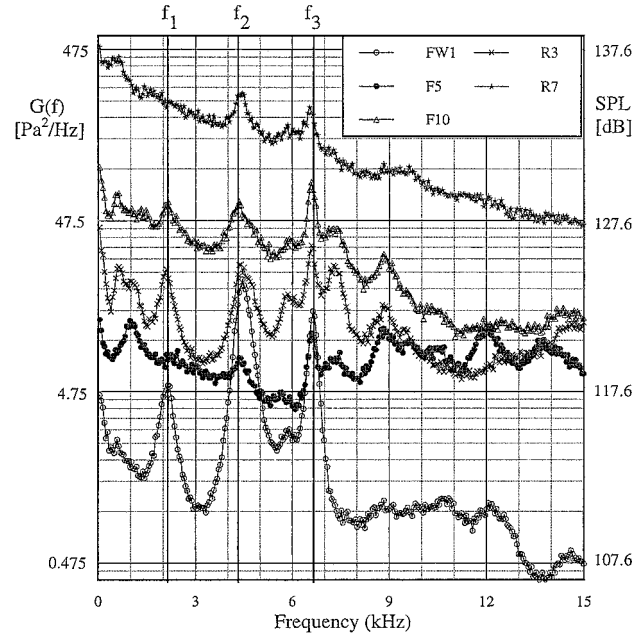

Fig. 8 Power spectra: baseline cavity, *L/H* = 3.

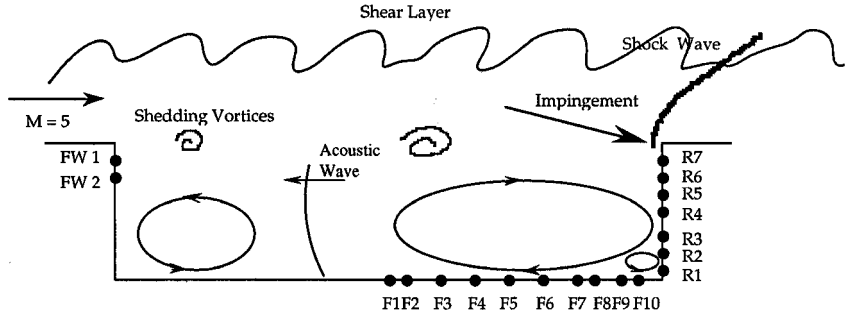

Fig. 7 Transducer port locations and inferred flow structure, *L/H* = 4.

Table 2 Experimental and calculated mode frequencies for $M = 4.95$

	$L/H=3$				$L/H=4$			
Prediction method	$n=1$	$n=2$	$n=3$	$n=4$	$n=1$	$n=2$	$n=3$	$n=4$
Strouhal number (measured)	0.21	0.43	0.66	0.88	0.22	0.42	0.71	0.95
Eq. (2), $r=1$ (closed box)	0.24	0.49	0.73	0.98	0.24	0.49	0.73	0.98
Eq. (1), $r=1$								
Rossiter,[23] $\alpha=0.25$								
$k_c=0.57$	0.20	0.46	0.73	0.99	0.20	0.46	0.73	0.99
$k_c=0.9$	0.24	0.56	0.87	1.19	0.24	0.56	0.87	1.19
Bauer and Dix,[27] α (linear)								
$k_c=0.7044, \alpha=0.21$	0.23	0.52	0.81	1.10				
$k_c=0.90, \alpha=0.21$	0.25	0.57	0.89	1.20				
$k_c=0.7044, \alpha=0.27$	——	——	——	——	0.21	0.52	0.81	1.10
$k_c=0.90, \alpha=0.27$	——	——	——	——	0.23	0.55	0.87	1.18
Eq. (1), $r=0.89$								
Heller and Bliss,[8] $\alpha=0$								
$k_c=0.47$	0.23	0.47	0.70	0.94	0.23	0.47	0.70	0.94
$k_c=0.9$	0.31	0.62	0.93	1.23	0.31	0.62	0.93	1.23

In Eq. (1), M is the freestream Mach number, γ is the specific heat ratio of the gas, and k_c is the ratio of the average vortex convection speed to the freestream flow speed. Although evaluation of the accuracy of Rossiter's formula is not the primary focus of the current work, it is worth examining how well it performs at Mach 5 for several reasons. Not the least of these is a remark made by Tam and Block[24] more than 20 years ago that "in the model a good deal of significance is attached to the highly localized vortices" yet schlieren photographs taken by Krishnamurty[25] and by Heller et al.[26] "did not indicate the presence of these vortices during cavity oscillations." Tam and Block[24] concluded that "vortex shedding is probably not important over the entire Mach number range as far as cavity oscillations are concerned." Some support for that view comes from the most recent experiments of Unalmis et al.[22] in which planar laser scattering (PLS) methods have been used in the same facility under the same incoming flow conditions as the present experiments but with a longer cavity ($L/H = 6$–8). Instantaneous PLS images showed no evidence for coherent structures induced by the cavity acoustics. Furthermore, ensemble-averaged velocity profiles in the shear layer, obtained using particle image velocimetry and conditioned on the upstream wall pressure, showed no evidence for deflection of the shear layer at different phases of the oscillation cycle. Overall the results suggested substantially less coupling between the cavity acoustics and the shear-layer fluid dynamics as compared to similar flows at lower Mach numbers. A consequence of less coupling, as will be shown subsequently, is that the acoustic modes can be calculated quite accurately without recourse to a flow model based on a vortex train.

A key question in using Rossiter's equation[23] is what values should be used for α and k_c. The dependence of α and k_c on flow conditions and L/H is discussed in some detail by Bauer and Dix[27] and by Perng.[3] Bauer and Dix,[27] fitted Rossiter's values,[23] of α (obtained in the Mach number range 0.4–1.2) to linear and second-order curves in terms of L/H. For $L/H = 3$ and 4 the linear fit gives $\alpha = 0.21$ and 0.27 respectively. Bauer and Dix,[27] also noted that a value of 0.57 has been accepted for k_c by several investigators, although East[28] had suggested it could be as high as 0.65. They[27] also point out that the value of 0.57 is, strictly speaking, restricted to a thin initial boundary layer, which is not the case for the current experiment. They attempted to include the effect of an initial boundary layer by assuming that the vortices moved at the velocity of the dividing streamline. This approach resulted in an expression for k_c, whose leading term is the theoretical incompressible value of 0.6163, which is then modified for compressibility by a term involving Mach number and a turbulent mixing position parameter. At $M_\infty = 4.95$, the expression gives an upper bound for $k_c (\leq 0.7044)$. Perng,[3] reviewed the work of Zhang and Edwards,[29] Maciulaitis,[30] and Rossiter,[23] spanning the Mach number range from 0.4 to 2.5 and noted that the suggested values of k_c ranged up to 0.75. Recent experimental results of Unalmis et al.[31] suggest it could be even higher. Based on double-pulse PLS images, it would appear that values of k_c could be as high as 0.9. Thus, it is far from clear what values of k_c and α should be used. Accordingly, Table 2 shows predictions for several combinations of k_c and α, as well as predictions based on closed-box acoustic modes. In this case, the resonance frequencies are given by $f_L = (a_0/2L) \times n$, where $n = 1, 2, 3, \ldots$. The corresponding Strouhal number where $n = 1, 2, 3, \ldots$, is

$$\frac{f_L L}{U_\infty} = \frac{\left[1 + (r/2)(\gamma - 1)M_\infty^2\right]^{\frac{1}{2}}}{2M_\infty} \times n, \qquad (2)$$

As noted by Unalmis et al.,[31] Table 2 shows that the closed-box acoustic modes are "often in better or equal agreement with the measured values compared to those predicted by the models." Unalmis et al. also reexamined the data of Clark et al.[11] and Bauer and Dix[27] and, consistent with the findings of Heller et al.,[26] found that as Mach number increases, the measured resonance frequencies approach the closed-box acoustic modes. These results provide support for the conclusions of Tam and Block[24] mentioned earlier. The lack of coupling has important implications for pressure oscillation suppression, the focus of this study. It seems unlikely (for a fixed length cavity) that mode frequencies can be altered; thus, successful suppression techniques will likely be those that limit the amount of mass entering the cavity.

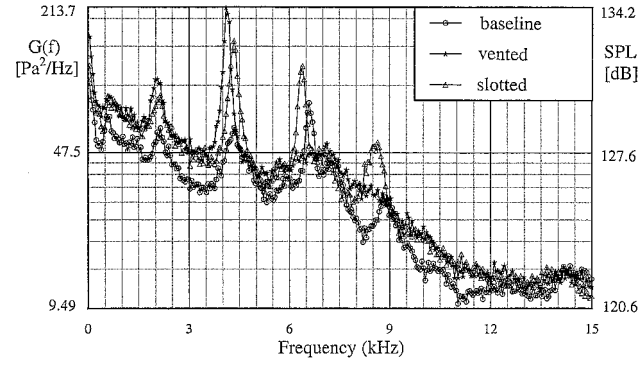

Fig. 9 Power spectra on cavity floor (port F10): baseline, slotted, and vented walls, $L/H = 3$.

Effects of Geometry Changes

The effectiveness of the various geometries has been assessed through their effects on the distributions of mean pressure, standard deviation, and OASPL and on the power spectra. Power spectra at transducer port F10 for the baseline and for the vented and slotted geometries as upstream walls are shown in Fig. 9 for $L/H = 3$. Transducer port F10, at $(x + y)/H = 2.81$, is close to the downstream wall/floor junction and is where the highest amplitude floor pressure oscillations occur. Vented and slotted upstream walls are

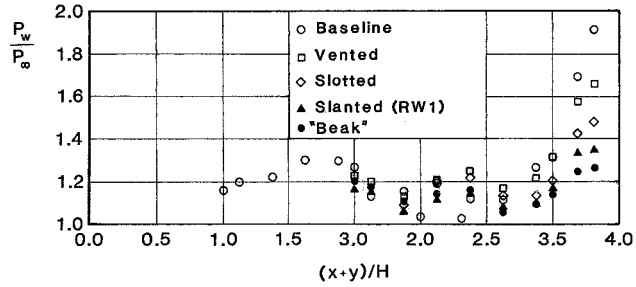

Fig. 10 Mean wall pressure distributions: baseline case and various downstream walls, $L/H = 4$.

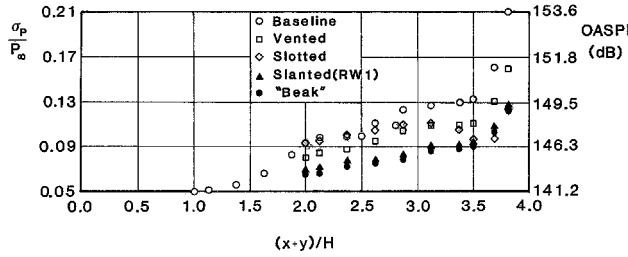

Fig. 11 Normalized wall pressure standard deviation and OASPL distributions: baseline case and various downstream walls, $L/H = 4$.

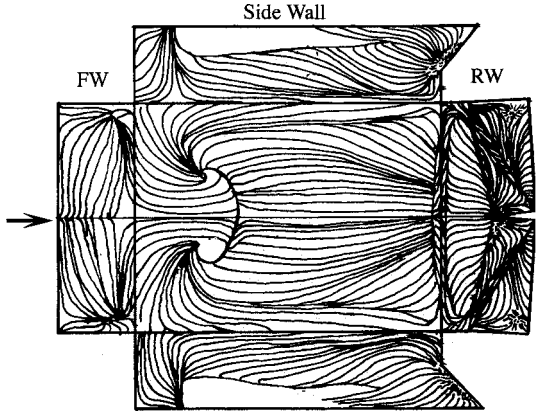

Fig. 12 Surface flow visualization with beak downstream wall, $L/H = 4$: exploded view.

clearly ineffective at suppressing the pressure oscillations. The amplitudes of the first and second modes are increased above baseline values, and the SPL at virtually all frequencies is increased. The vented upstream wall seems to eliminate the third mode, but the reasons why are not known. Based on these results, attention was refocused on the downstream wall.

Normalized mean wall pressure distributions for the baseline, vented, slotted, slanted (RW1), and beak downstream walls are shown in Fig. 10 for $L/H = 4$. All four downstream walls lower the mean pressure near the floor/downstream wall junction below baseline values, with the slanted and beak downstream walls producing the largest reductions, approximately 30 and 35%, respectively, at the farthest downstream station. Figure 11 shows that the four downstream walls reduce fluctuation intensities on the cavity floor with the slanted and beak walls producing the largest reductions. At the station on the cavity floor closest to the downstream wall, the slanted and beak downstream walls both produce a reduction in rms fluctuation intensity of about 40%, corresponding to an OASPL reduction from approximately 154 to 149 dB. An exploded surface flow visualization for the beak downstream wall, for $L/H = 4$, is shown in Fig.12 and supplies some evidence as to why this geometry is effective. Although comparison with the baseline case (Fig. 6) shows that the overall structure is qualitatively similar, it is evident that on the downstream wall more mass flow is swept spanwise and out of the cavity reducing the intensity of the downstream vortex.

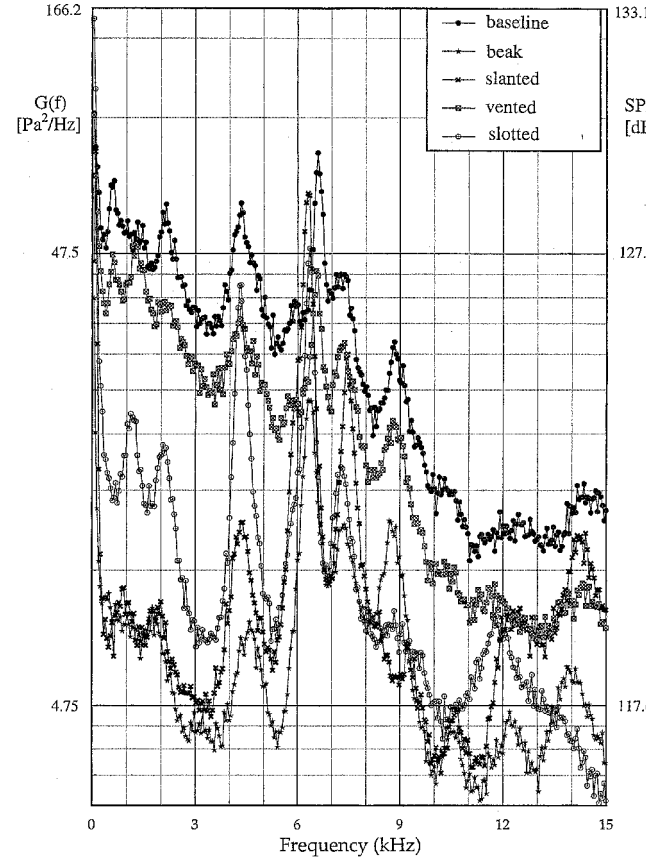

Fig. 13 Power spectra on cavity floor (port F10): baseline case and various downstream walls.

Power spectra for the same five cases as in Figs. 10 and 11 were obtained for both $L/H = 3$ and 4. Results for $L/H = 3$ are shown in Fig. 13. The data are all at port F10, at $(x + y)/H = 2.81$, which is close to the downstream wall/floor junction and is where the highest amplitude floor pressure oscillations occur. The slotted and vented downstream walls are not as effective as the slanted and beak walls, although as might be expected from Fig. 11, they do provide some alleviation. The vented downstream wall provides little attenuation of the first four modes at $L/H = 3$. At $L/H = 4$ (not shown), they are all attenuated by a factor of about 2. The slotted downstream wall is even more effective at attenuating the first and second modes at $L/H = 4$, whereas the third mode is essentially unaltered, and attenuation of the fourth mode is comparable to that of the vented wall. At $L/H = 3$, the first mode is similarly reduced, but the second (and third) modes are largely unaffected.

The slanted wall is far more effective than either the slotted or vented geometries. At $L/H = 3$, the first and second modes are attenuated by factors of 7–8 and about 5, respectively, although, as with the slotted and vented walls, the third mode is largely unaffected. At $L/H = 4$, the slanted wall is even more effective. Not only are the first and second modes attenuated by larger factors than at $L/H = 3$, but the third and fourth modes are attenuated by a factor of about 2. Note that because the downstream wall is slanted the effective cavity length is increased giving rise to slightly lower mode frequencies. Results for the beak downstream wall, swept in two directions, show that this geometry is even better than one with a streamwise inclination only. At $L/H = 3$, not only are the first and second modes attenuated by factors of about 8 (similar to the slanted wall), but the amplitude of the third mode (the strongest mode at $L/H = 3$) is reduced by a factor of 3–4. At $L/H = 4$, attenuation of the first and second modes is larger (about 10 and 20, respectively), whereas that of the third (and fourth) mode is about the same.

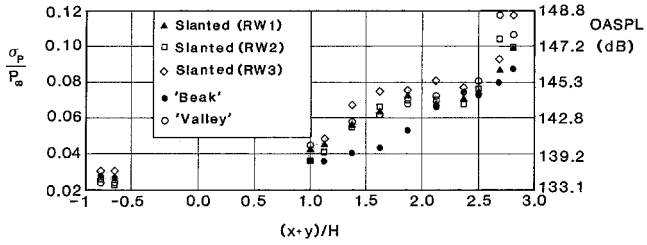

Fig. 14 Normalized wall pressure standard deviation and OASPL distributions: baseline case and various downstream walls, $L/H = 3$.

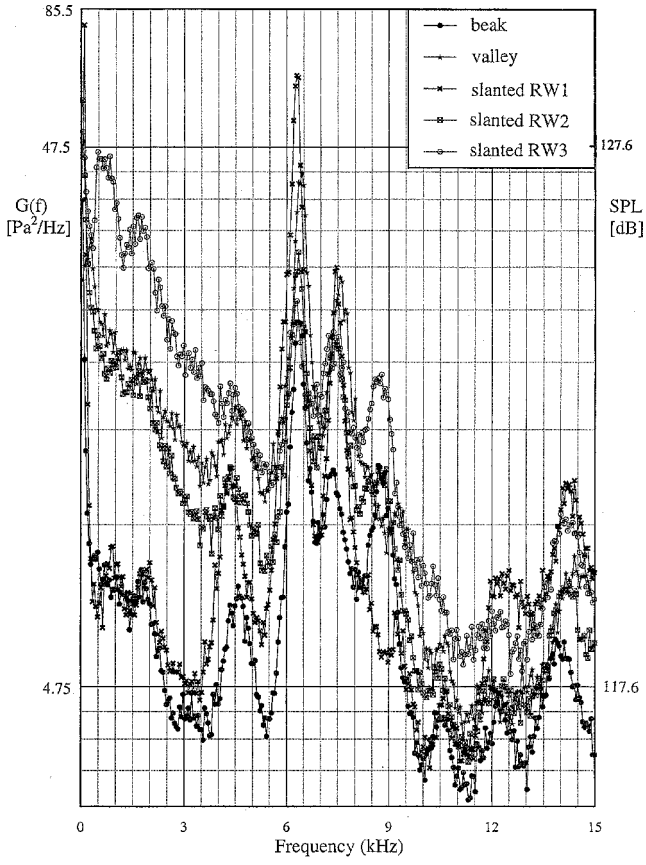

Fig. 15 Power spectra on cavity floor (port F10): beak, valley, and slanted downstream walls.

Of the four described downstream walls, the beak was the most effective overall, although the 45-deg inclined wall came close. Because the inclination angle of the latter had been selected arbitrarily, two additional walls were tested with angles of 38.7 and 30.2 deg. As mentioned earlier, the inclined surfaces of the latter extend farther into the cavity than with a 45 deg surface. In addition, largely out of curiosity, the valley downstream wall was also tested; in this case (Fig. 2e) the centerline is cut deeper than the edges. Figure 14 shows the normalized rms pressure fluctuation level and SPL for the beak, the valley, and the three slanted downstream walls. All geometries reduce the fluctuation intensity below the baseline case with the beak downstream wall providing the largest reduction. Over most of the cavity floor, slant angles of 45 and 38.7 deg generate essentially the same result, whereas a reduction in angle to 30.2 deg increases the intensity by around 10%.

Power spectra for these same cases are shown in Fig. 15 for $L/H = 3$ and Fig. 16 for $L/H = 4$. The data are close to the downstream wall/floor junction at stations $(x + y)/H = 2.81$ and 3.81, respectively. When the beak results are used as a reference, the valley and slanted walls RW2 and RW3 enhanced the second, third, and fourth modes by factors of 1.4–2.5 at $L/H = 3$ and were not overall an improvement over the original slanted wall RW1. The valley and slanted wall RW2 enhanced the first, third, and fourth modes by

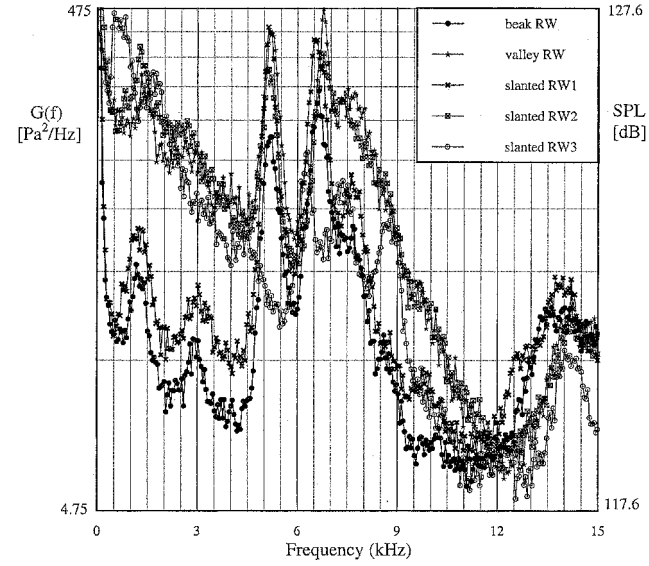

Fig. 16 Power spectra on cavity floor (port F10): beak, valley, and slanted downstream walls, $L/H = 4$.

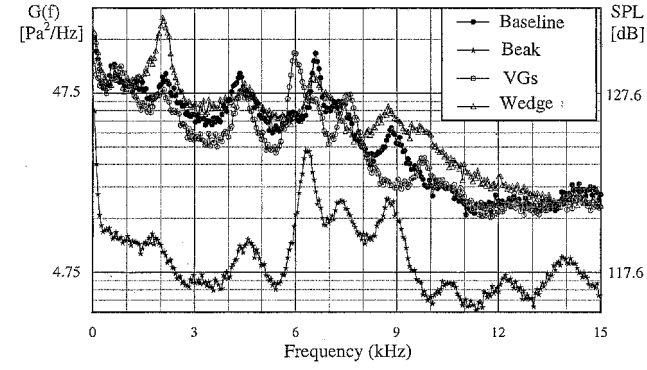

Fig. 17 Power spectra on cavity floor (port F10) with boundary-layer spoilers, $L/H = 3$.

factors ranging from about 1.2 to 2.7 at $L/H = 4$. No obvious peak occurred around the second mode. Wall RW3 enhanced the first and second modes by a factor of about 4, and the first mode became the strongest mode. Overall, the beak wall is clearly the most effective. In addition to the significant OASPL reduction at all stations on the floor, it attenuated the strongest (third) mode at $L/H = 3$ by a factor of 3.5. The corresponding factors for RW2, RW3, and the valley walls were 2.6, 2.2, and 1.9, respectively. At $L/H = 4$, the strongest (second) mode was attenuated by a factor of 7 using the beak wall compared to 3.7 (wall RW3), 5.5 (wall RW2), and 4.6 (valley wall).

Power spectra at station F10, at $(x + y)/H = 2.81$ and at the top of the downstream wall, at $(x + y)/H = 3.87$, with vortex generators and wedge separator upstream of the cavity, are shown in Figs. 17 and 18, respectively, for $L/H = 3$. Results for the baseline and beak downstream wall cases are also included in Fig. 17. No beak data are available on the downstream wall itself and so Fig. 18 includes only the baseline data. The vortex generators have little effect at transducer port F10. There is a modest attenuation of the first and second modes, but the third mode is almost unchanged. The wedge attenuates the third mode a little, leaves the second almost unchanged, but amplifies the first by a factor of 2.3. On the downstream wall, both spoiler geometries enhance the power levels significantly. The vortex generators and wedge enhance the second mode by factors of 6 and 2 and the third mode by factors of 7 and 1.5, respectively. Inspection of the pressure signals on the downstream wall at ports R7 and R6 indicate that the spoilers cause the shear layer to deflect deeper into the cavity. Thus, the intermittent pressure signals of the type seen in Fig. 5 are enhanced when spoilers are employed.

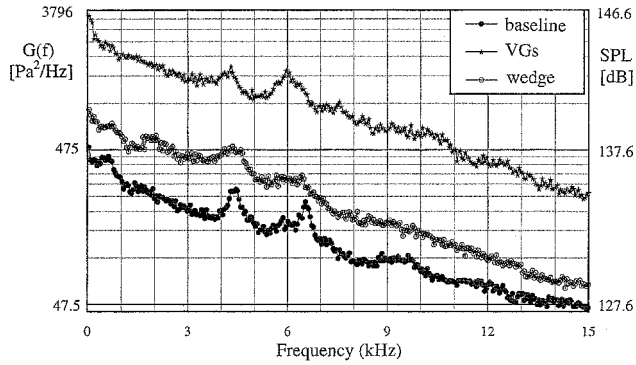

Fig. 18 Power spectra on cavity downstream wall (port R7) with boundary-layer spoilers, $L/H = 3$.

Discussion and Summary

In a given application the choice of internal wall geometry will be dictated by many constraints. It may be necessary to attenuate the amplitude of a specific mode, in which case a geometry which is most effective in a narrowband may be preferable to one that is effective over a broadband. Thus, it is difficult, and probably not meaningful, to claim that one particular geometry is the most effective. However, some broad conclusions can be drawn from the current work, which should offer some useful guidance and help to decide on a starting point for a more focused computational or experimental study. These data should also prove useful in assessing whether computational methods (in particular the growing body of work using LES) can not only reproduce the fluctuation intensities for a given geometry, but can accurately model the systematic effects of geometry changes for fixed external flow conditions.

Consistent with earlier work at lower Mach numbers, an inclined downstream wall can be quite effective. Although the beak wall that is swept both streamwise and spanwise appears to be the most effective, a simpler geometry that is swept in the streamwise direction only is also very effective. Although downstream wall sweep does not change the basic cavity flow structure (based on surface flow visualization and the shapes of the mean and rms pressure distributions) or change the mode frequencies (which for given flow conditions depend primarily on cavity length), the reduction in mass flow into the cavity weakens the downstream vortex significantly. By the use of either the beak wall or the 45-deg inclined wall, rms pressure fluctuation intensities near the downstream wall/floor junction (the site of the most intense fluctuations on the floor) were reduced by about 40%. At stations on the cavity floor, at the midpoint, reductions of around 20% were obtained, indicating that the effect is not just local. These geometries are also generally quite effective at attenuating the cavity modes. For example, at $L/H = 4$, the beak wall reduces the amplitude of the first and second modes by factors of about 10 and 20, respectively, and the third mode (the strongest mode) by a factor between 3 and 4.

Acknowledgments

Support for this work has been provided through Grant F49620-95-1-1001 from the Air Force Office of Scientific Research monitored initially by L. Sakell and subsequently by S. Walker. The authors gratefully acknowledge this support. Additional funding for support of the first author was provided by the government of the Republic of China.

References

[1]Charwat, A. F., Roos, J. N., Dewey, F. C., Jr., and Hitz, J. A., "An Investigation of Separated Flows—Part I: the Pressure Field," *Journal of the Aerospace Sciences*, Vol. 28, No. 6, 1961, pp. 457–470.

[2]Rockwell, D., and Naudascher, E., "Review—Self-Sustaining Oscillations of Flow Past Cavities," *Journal of Fluids Engineering.*, Vol. 100, No. 2, 1978, pp. 152–165.

[3]Perng, S. W., "Passive Control of Pressure Oscillations in Hypersonic Cavity Flow" Ph.D. Dissertation, Dept. of Aerospace Engineering and Engineering Mechanics, Univ. of Texas, Austin, TX, Dec. 1996.

[4]Rizetta, D. P., "Numerical Simulation of Supersonic Flow Over a Three-Dimensional Cavity," *AIAA Journal*, Vol. 26, No. 7, 1988, pp. 799–807.

[5]Vakili, A. D., and Gauthier, C., "Control of Cavity Flow by Upstream Mass Injection," *Journal of Aircraft*, Vol. 31, No. 4, 1994, pp. 169–174.

[6]Vakili, A. D., Wolfe, R., Nagle, I., and Lambert, E., "Active Control of Cavity Aeroacoustics in High Speed Flows," AIAA Paper 95-0678, 1978.

[7]Sarno, R. L., and Franke, M. E., "Suppression of Flow-Induced Pressure Oscillations in Cavities," *Journal of Aircraft*, Vol. 31, No. 1, 1994, pp. 90–96.

[8]Heller, H. H., and Bliss, D. B., "The Physical Mechanism of Flow-Induced Pressure Fluctuations in Cavities and Concepts for Their Suppression," AIAA Paper 75-491, 1975.

[9]Baysal, O., and Stallings, R. L., Jr., "Computational and Experimental Investigation of Cavity Flowfields," *AIAA Journal*, Vol. 26, No. 1, 1988, pp. 6, 7.

[10]Wilcox, F. J., Jr., "Passive Venting System for Modifying Cavity Flowfields at Supersonic Speeds," *AIAA Journal*, Vol. 26, No. 3, 1988, pp. 374–376.

[11]Clark, R. L., Kaufman, L. G., II, and Maciulaitis, A., "Aeroacoustic Measurements for Mach 0.6–3.0 Flows Past Rectangular Cavities," AIAA Paper 80-0036, 1980.

[12]Shaw, L. L., Clark, R., and Talmadge, D., "F-111 Generic Weapons Bay Acoustic Environment," *Journal of Aircraft*, Vol. 25, No. 2, 1988, pp. 147–153.

[13]Smith, R. A., Gutmark, E., and Schadow, K. C., "Mitigation of Pressure Oscillations Induced by Supersonic Flow over Slender Cavities," AIAA Paper 90-4019, 1990.

[14]Sinha, N., Dash, S. M., Chidambaram, N., and Findlay, D., "A Perspective on the Simulation of Cavity Aeroacoustics," AIAA Paper 98-0286, Jan. 1999.

[15]Rockwell, D., and Knisely, C., "The Organized Nature of Flow Impingement upon a Corner," *Journal of Fluid Mechanics*, Vol. 93, Pt. 3, 1979, pp. 413–432.

[16]Zhang, X., "An Experimental and Computational Investigation into Supersonic Shear Layer Driven Single and Multiple Cavity Flowfields," Ph.D. Dissertation, Dept. of Engineering, Univ. of Cambridge, Cambridge, England, U.K., Feb. 1987.

[17]Suhs, N. E., "Computational of 3-D Cavity Flow at Subsonic and Supersonic Mach Numbers," AIAA Paper, 87-1208, 1987.

[18]Baysal, O., Yen, G.-W., and Fouladi, K., "Navier–Stokes Computations of Cavity Aeroacoustics with Suppression Devices," *Journal of Vibration and Acoustics*, Vol. 116, No. 1, Jan. 1994, pp. 105–112.

[19]Wheeler, G. L., "Means for Maintaining Attached Flow of a Flowing Medium," U.S. Patent 4,455,045, Filed June 19, 1984.

[20]Barter, J. W., "Prediction and Passive Control of Fluctuating Pressure Loads Produced by Shock-Induced Turbulent Boundary Layer Separation," Ph.D. Dissertation, Dept. of Aerospace Engineering and Engineering Mechanics, Univ. of Texas, Austin, TX, Dec. 1995.

[21]Unalmis, O. H., Clemens, N. T., and Dolling, D. S., "Planar Laser Imaging of a Supersonic Side-Facing Cavity," AIAA Paper 99-1297, 1999.

[22]Unalmis, O. H., Clemens, N. T., and Dolling, D. S., "Planar Laser Imaging of High Speed Cavity Flow Dynamics," AIAA Paper 99-0776, 1998.

[23]Rossiter, J. E., "Wind-Tunnel Experiments on the Flow over Rectangular Cavities at Subsonic and Transonic Speeds," Aeronautical Research Council Rept. and Memoranda ARCR & M 3438, London, 1964.

[24]Tam, C. K. W., and Block, P. J. W., "On the Tones and Pressure Oscillations Induced by Flow over Rectangular Cavities," *Journal of Fluid Mechanics*, Vol. 80, Pt. 2, 1978, pp. 373–399.

[25]Krishnamurty, K., "Acoustic Radiation from Two-Dimensional Rectangular Cutouts in Aerodynamic Surfaces," NACA-TN-3487, Aug. 1955.

[26]Heller, H. H., Holmes, D. G., and Covert, E. E., "Flow-Induced Pressure Oscillations in Shallow Cavities," *Journal of Sound and Vibration*, Vol. 18, No. 4, 1971, pp. 545–553.

[27]Bauer, R. C., and Dix, R. E., "Engineering Model of Unsteady Flow in a Cavity," Arnold Engineering Development Center, Arnold Air Force Base, Tennesse, AEDC-TR-91-17, Dec. 1991.

[28]East, L. F., "Aerodynamically Induced Resonance in Rectangular Cavities," *Journal of Sound and Vibration*, Vol. 3, No. 3, 1966, pp. 277–287.

[29]Zhang, X., and Edwards, J. A., "An Investigation of Supersonic Oscillatory Cavity Flows Driven by Thick Shear Layers," *Aeronautical Journal*, Vol. 16, No. 940, Dec. 1990, pp. 355–364.

[30]Maciulaitis, A., "Improved Prediction of Frequency Modes for Peak Amplitude Pressures in Simulated Bomb Bays at Mach 0.6 to 3.0," Research Dept. Memorandum RM-708, Grumman Aerospace Corp., Bethpage, NY, June 1980.

[31]Ünalmis, O. H., Clemens, N. T., and Dolling, D. S., "Experimental Study of Shear-Layer/Acoustics Coupling in Mach 5 Cavity Flow," *AIAA Journal*, Vol. 39, No. 2, 2001, pp. 242–252.